Symmetry-driven phonon chirality and transport in one-dimensional and bulk Ba_{3}N-derived materials

Tribhuwan Pandey, Carlos A. Polanco, Valentino R. Cooper, David S. Parker, and Lucas Lindsay

Phys. Rev. B **98**, 241405 — Published 4 December 2018

DOI: 10.1103/PhysRevB.98.241405

Symmetry-driven phonon chirality and transport in 1D and bulk Ba_3N-derived materials

Tribhuwan Pandey, Carlos A. Polanco, Valentino R. Cooper, David S. Parker, and Lucas Lindsay

Materials Science and Technology Division, Oak Ridge National Laboratory, Oak Ridge, TN 37831 USA

Symmetry-driven phonon chirality and transport in 1D and bulk Ba_3N-derived materials

Tribhuwan Pandey, Carlos A. Polanco, Valentino R. Cooper, David S. Parker, and Lucas Lindsay

Materials Science and Technology Division, Oak Ridge National Laboratory, Oak Ridge, TN 37831 USA

Abstract: Symmetry and dimensionality are essential factors defining lattice dynamics and conductivity (κ). Here, we critically examine these via *ab initio* Boltzmann transport applied to single chain and bulk electride Ba_3N and Ba_3NX (X=Sb,Bi). Chiral phonons in 1D chains obey new symmetry-based scattering rules that limit thermal resistance. Weak chain coupling breaks these in the bulk, giving lower κ and large κ anisotropy. Curiously, intercalation of large X atoms binds chains more strongly, reducing the volume, yet gives lower κ and transforms the electronic behavior. Insights developed here can be more generally applied to other materials and provide novel avenues for predictive materials design.

Key words: One-dimensional transport, thermal transport anisotropy, Boltzmann transport theory, phonon anharmonicity, interaction selection rules

Introduction — Weakly bonded and low-dimensional materials have emerged as a cornerstone for modern opto- and nano-electronic devices, including electronic and thermal interconnects, solar cells, lasers, thermoelectrics and thermal management materials [1-5]. Lattice thermal conductivity (κ), a critical property for these applications, depends on material composition, structure, symmetry and dimensionality. High power devices require materials with high κ, while thermoelectric devices require materials with low κ and superior electronic properties. These thermal transport extremes are often found in layered materials, which exhibit anisotropy in conductivity due to their structure and bonding. Higher κ is observed along directions of strong covalent bonding, while lower κ manifests along directions of weaker bonding. The prototypical example is graphite with van der Waals (vdW) bonded carbon layers, for which the basal plane κ is ~2000 $Wm^{-1}K^{-1}$, while the value across the layers is 6 $Wm^{-1}K^{-1}$ [6-8]. Similarly, the in-plane κ for bulk MoS_2 ranges from 85-112 $Wm^{-1}K^{-1}$ [9,10], 15-30 times higher than the cross-plane values [11]. These weakly bonded structures provide avenues for tuning κ by varying layer number [9], applying strain [12,13] and intercalating atoms between layers [14-16].

Similar to layered 2D materials, 1D chains can be weakly bonded to form bulk materials (e.g., TiS_3 [17,18] and $TaSe_3$ [19,20]) with highly anisotropic thermal transport nearly confined to a single direction. While thermal transport in 2D materials has been explored intensively [6,21-26], transport in quasi-1D materials has been little studied, with the exception of polyethylene chains [27], Mn_nSi_{2n-m} [28], and $Ta_2Pd_3Se_8$ nanowires [29].

In this rapid communication, we investigate how composition, structure, symmetry and dimensionality govern κ behavior in single chain and weakly bonded quasi-1D systems of the proposed electride Ba_3N [30] and related systems. In particular, we employ the Boltzmann transport equation (BTE) methodology coupled with density functional theory (DFT) to describe the electronic structure, phonon scattering and transport properties of an isolated single chain of Ba_3N, bulk Ba_3N (vdW

coupled chains) and bulk Ba_3NX (X=Sb,Bi) (see **Figure 1** for structures). We describe phonon chirality[31-33] and symmetry selection rules for phonon-phonon interactions in the 1D Ba_3N chain, thereby obtaining scattering rules that apply to a general class of 1D systems. These selection rules are partly responsible for an unusual contribution to κ by high frequency optical phonons and a substantial variation in κ behavior in going from 1D to 3D Ba_3N. We examine the κ anisotropy in bulk Ba_3N ($\kappa_z / \kappa_x \sim 7.5$ at room temperature (RT=300K), where z is along the chains and x is perpendicular) and Ba_3NX, and demonstrate an unusual competition between structure and scattering to determine κ when introducing heavy Sb or Bi atoms to the Ba_3N chain lattice. Lastly, we discuss the electronic properties of these materials, namely, that despite their similar crystal structures, Ba_3N is metallic, while Ba_3NSb and Ba_3NBi are semiconductors with bandgaps ~0.5-0.6 eV.

Single chain Ba_3N — Structural symmetries play a governing role in vibrational properties, phonon interactions and lattice transport, particularly in lower dimensional materials. Single chain Ba_3N is built from units of 3 Ba atoms that form an equilateral triangle (edge length 3.642 Å) with an N atom centrosymmetric above it at a distance $c/4$ where c = 7.050 Å, as shown by the gray square in **Figure 1(a)**. The unit cell that describes the chain is composed of two such units, one located $c/2$ above the other and rotated by π (dashed rectangle in **Figure 1(a)** gives the side view). These alternating rotated units are stacked on each other to create the Ba_3N chain which we define to lie along the z axis. The rotational symmetry between these building blocks within the unit cell yields a description of the lattice dynamics within the smaller symmetry-reduced cell (1 N and 3 Ba atoms) with a rotation operator ($S^l_{\alpha\beta}$) and lattice vectors $\vec{R}_l = (R_{lz}, \theta_l)$, where R_{lz} locates the symmetry-reduced cell along the chain. For cells located at $R_{lz} = nc$ with n an integer, $\theta_l = 0$ and $S^l_{\alpha\beta}$ is the identity matrix, while for cells located at $R_{lz} = c(n+1/2)$ $\theta_l = \pi$ and $S^l_{\alpha\beta}$ is a π-rotation matrix. The dynamical matrix that describes the vibrations of the chain is then given by [34,35]:

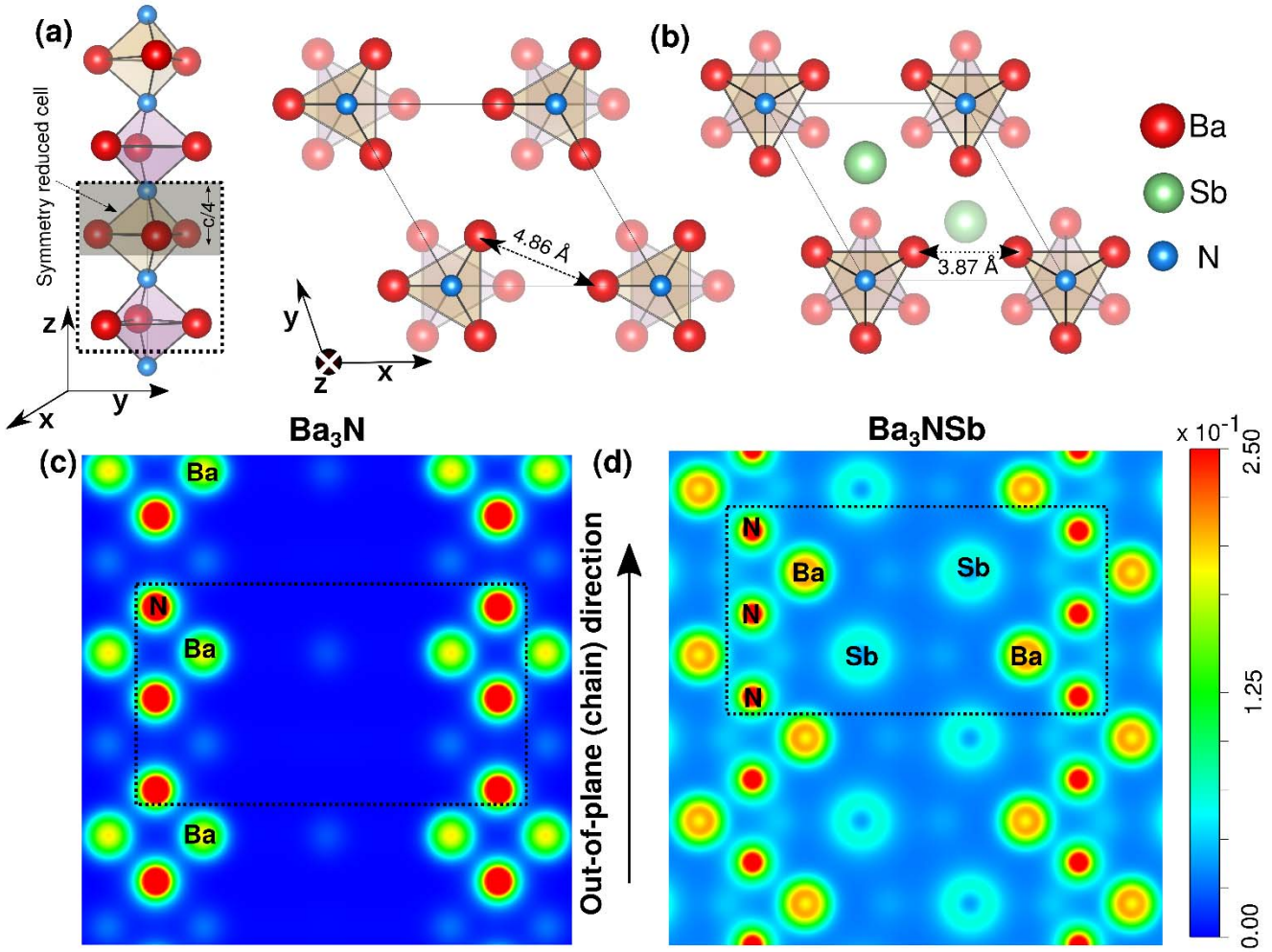

Figure 1: Structure of (a) Ba_3N and (b) Ba_3NSb as viewed in the *xy* plane. A side view of an isolated Ba_3N chain is also shown in (a). Charge density for (c) Ba_3N and (d) Ba_3NSb projected in the (110) plane. For bulk Ba_3N the chains are nearly isolated, while for Ba_3NSb the chains interact via Sb atoms. The unit cell of single chain Ba_3N is illustrated by dashed black lines, while the symmetry-reduced four atom unit is highlighted by the gray rectangle in (a). The crystal structure of Ba_3NBi is similar to Ba_3NSb.

$$D_{\alpha\beta}^{kk'}(q_z\ell)=\frac{1}{\sqrt{m_k m_{k'}}}\sum_{l'}\sum_{\gamma}\Phi_{\alpha\gamma}^{0k,l'k'}S_{\gamma\beta}^{l'}e^{i(q_z R_{l'z}+\ell\theta_{l'})}$$

(1)

where q_z is a continuous wavevector along the chain, m_k is the mass of the k^{th} atom, $\Phi_{\alpha\beta}^{0k,l'k'}$ is the harmonic interatomic force constant (IFC) between the k^{th} atom in the 0^{th} cell and the k'^{th} atom in the l'^{th}

cell for the α^{th} and β^{th} directions. Cells here are now composed of the smaller four atom units. The phonon modes pick up a rotational quantum number $\ell = 0, 1$, or chirality, which leads to conservation conditions for three-phonon scatterings (described below). This chirality is likely present in a wide array of single chain systems (e.g., polyethylene), and measurement [31] and utilization of this phonon chirality may be possible in novel quantum applications.

Diagonalization of Eq. 1 for every q_z and ℓ gives the 1D phonon dispersion for the Ba_3N chain, which is compared with its 3D bulk counterpart in **Figures 2(a) and 2(b)**. Twelve red curves correspond to phonon branches with chirality $\ell = 0$, and twelve blue curves for $\ell = 1$. The Ba_3N chain demonstrates typical low-frequency acoustic phonon behavior having two quadratic flexure branches, one linear longitudinal (LA) branch and one linear torsional branch. These correspond to rigid *x*, *y*, *z* crystal translations and a rotation about the chain axis, respectively. The quadratic flexure branch behavior is common in low dimensional materials like nanotubes[36], 1D polyethylene chains[37] and graphene[38].

As previously demonstrated with single-walled carbon nanotubes[34,39], the ℓ chirality must be conserved in a phonon-phonon scattering process, independent of the number of phonons involved. Thus, the conservation of momentum and energy conditions for three-phonon scatterings are given by:

$$\begin{aligned} \ell \pm \ell' &= \ell'' + \ell_G \\ q_z \pm q_z' &= q_z'' + G_z \\ \omega_{q_z \ell j} \pm \omega_{q_z' \ell' j'} &= \omega_{q_z'' \ell'' j''} \end{aligned} \tag{2}$$

where $\omega_{q_z \ell j}$ is the phonon frequency for phonon with q_z and ℓ in the j^{th} branch, and G_z and ℓ_G are components of the reciprocal lattice vector. $G_z = 2\pi n / c$ and $\ell_G = m$ with *n* and *m* non-zero integers for Umklapp processes, and *n*=*m*=0 for Normal processes. This added quantum conservation condition restricts how three phonons can interact compared with bulk Ba_3N and contributes to reduced thermal resistance in the chain.

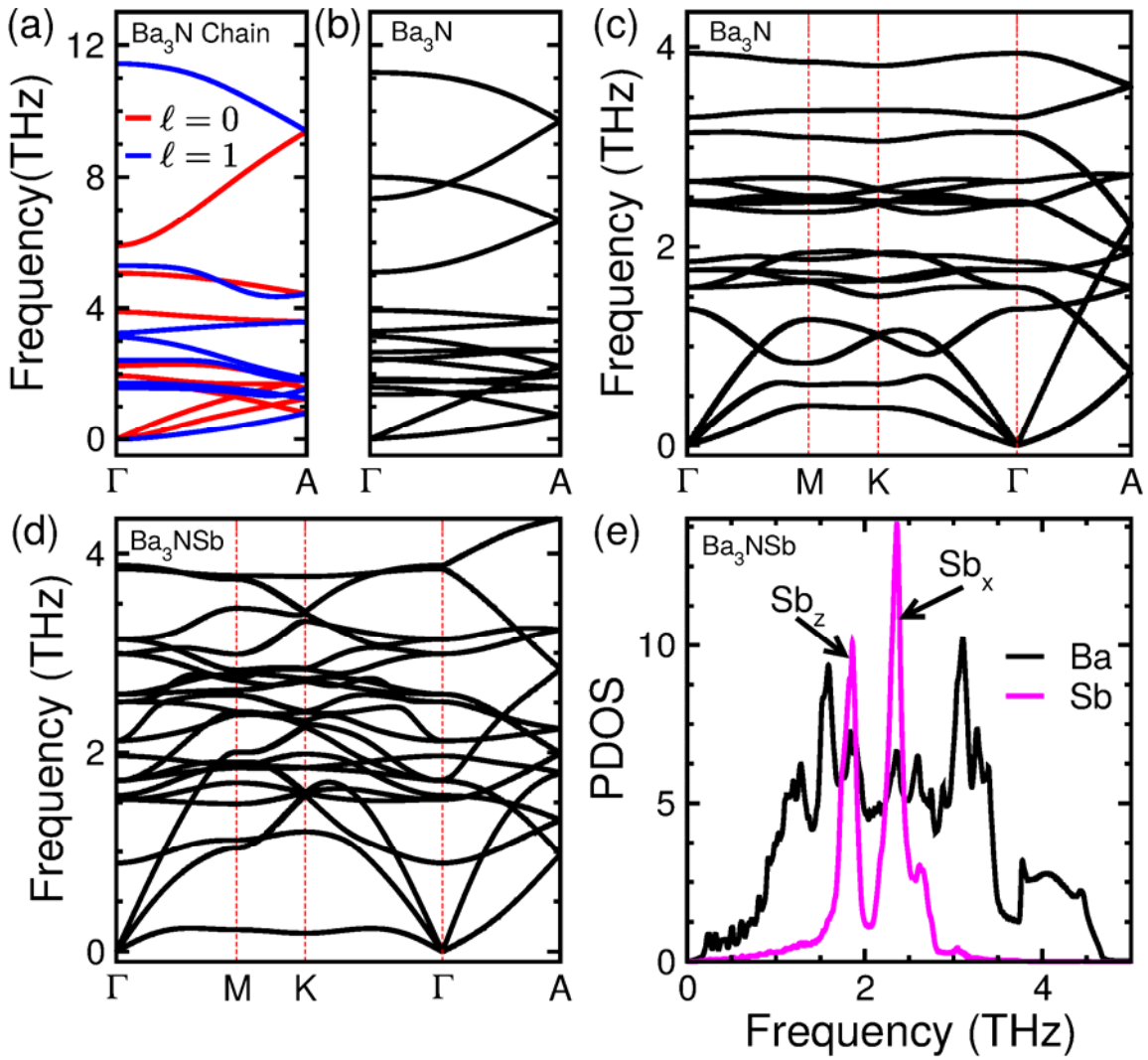

Figure 2: The full phonon dispersions for (a) single chain Ba_3N, (b) bulk Ba_3N along the out of plane direction. The phonon dispersion of single chain Ba_3N is decoupled in terms of the quantum number ℓ. The single chain flexure branches $(\ell = 1, j = 1)$ and $(\ell = 1, j = 2)$ are degenerate. Also shown are the low frequency phonon dispersions for(c) bulk Ba_3N and (d) Ba_3NSb along high symmetry directions. (d) Phonon density of states (PDOS) for Ba_3NSb.

Still another symmetry selection rule is present for the N atoms in the chain structure, which governs their vibrations and interactions. Neglecting high order anharmonic and trivial terms, the potential energy near equilibrium is given by:

$$V = \frac{1}{2}\sum_{\alpha\beta}\sum_{lkl'k'}\Phi_{\alpha\beta}^{lkl'k'}u_{\alpha}^{lk}u_{\beta}^{l'k'} + \frac{1}{6}\sum_{\alpha\beta\gamma}\sum_{lkl'k'l''k''}\Phi_{\alpha\beta\gamma}^{lkl'k'l''k''}u_{\alpha}^{lk}u_{\beta}^{l'k'}u_{\beta}^{l''k''} \quad (3)$$

where $\Phi_{\alpha\beta\gamma}^{lkl'k'l''k''}$ are the anharmonic IFCs that govern three-phonon interactions and u_{α}^{lk} is a small displacement of the k^{th} atom in the l^{th} cell in the α^{th} direction. Each term must satisfy the symmetry constraints imposed by the crystal. Thus, for one N atom displaced along *z*, the first term in Eq. 3 must be invariant to ± displacements perpendicular to *z* (e.g., u_{x}^{lk} and $-u_{-x}^{lk}$). This is similarly true for two N atoms displaced along the *z* direction in the second term of Eq. 3. Thus, for *k*=*k*'=*k*''=N, $\Phi_{xz}^{lkl'k'} = -\Phi_{xz}^{lkl'k'} = 0$ and $\Phi_{xzz}^{lkl'k'l''k''} = -\Phi_{xzz}^{lkl'k'l''k''} = 0$ and like terms. This leads to a decoupling of N vibrations parallel and perpendicular to the chain and limits the three-phonon scatterings available in the Ba_3N chain. Similar selection rules can be derived for higher order interactions. This symmetry selection rule is not as prohibitive as a similar reflection symmetry rule previously found in graphene [28], however, when coupled with the quantum selection rule in Eq. 2, this further limits the scattering resistance in the Ba_3N chain compared with that in bulk Ba_3N.

The calculated κ for single chain Ba_3N as a function of temperature is given in **Figure 3(a)** (also compared with bulk Ba_3N) and defined by:

$$\kappa_{\alpha} = \sum_{\vec{q}j} C_{\vec{q}j} v_{\vec{q}j\alpha}^{2} \tau_{\vec{q}j\alpha} \quad (4)$$

where $v_{\vec{q}j\alpha}$ is the α^{th} component of the velocity of phonon mode with wavevector $\vec{q}$ in branch *j*, $C_{\vec{q}j}$ is the volume-normalized mode specific heat, and $\tau_{\vec{q}j\alpha}$ is the transport lifetime, which is computed from the full solution of the BTE. For the Ba_3N chain, $\vec{q} = (q_z, \ell)$, *j*=1-12 and transport is along *z* only, while for bulk $\vec{q} = (q_x, q_y, q_z)$, *j*=1-24 and transport occurs along all three Cartesian directions with $\kappa_x = \kappa_y \neq \kappa_z$. DFT-based calculations of the vibrational and transport properties have been described previously [40-42]; calculation details specific to Ba_3N and Ba_3NX are given in the Supplemental Material [43]. Despite giving little thermal resistance, we have incorporated phonon-isotope scattering

from the natural isotope variations for each element [44,45]. As with other lower dimensional systems [6,30,40], the often-employed relaxation time approximation (RTA) [46] does not yield accurate results for the Ba_3N chain: $\kappa_{\text{full BTE}} / \kappa_{\text{RTA}} = 1.6$ at RT. Large integration meshes are required to get converged results for the 1D chain and special care was taken to describe the scattering of the ultralow frequency acoustic modes (see Supplemental Material for details [43]).

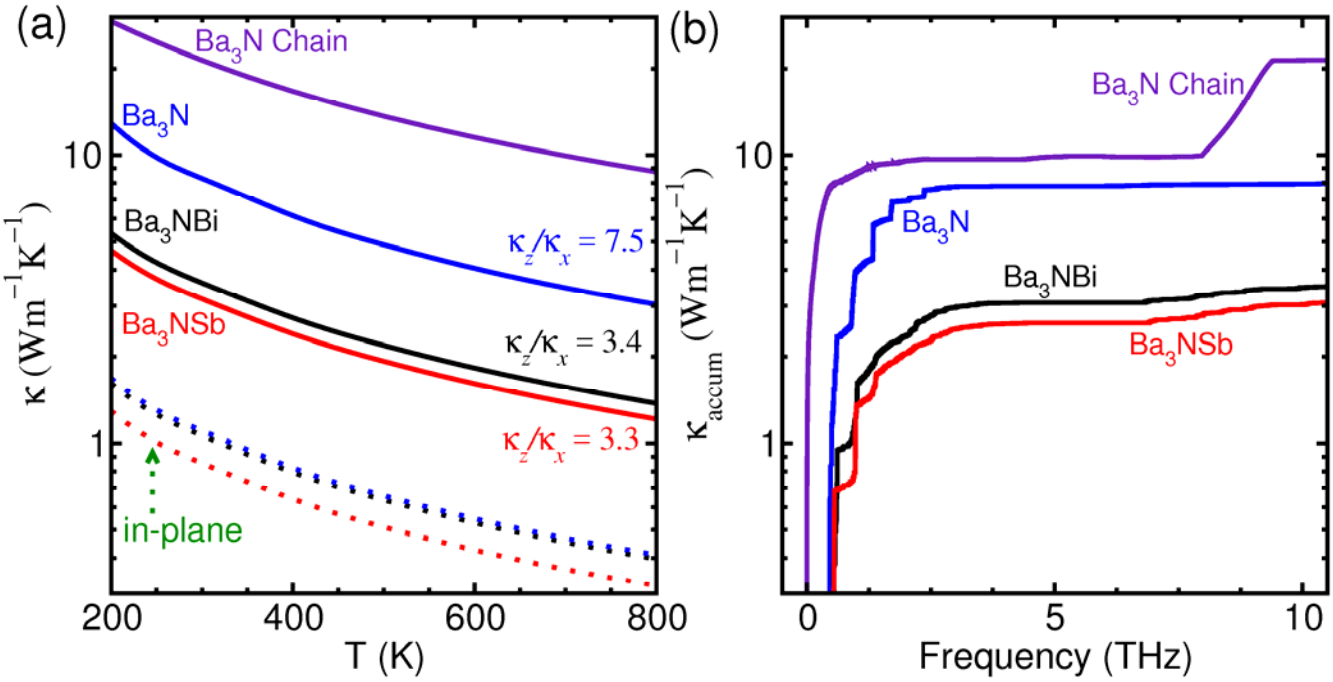

Figure 3: Calculated lattice thermal conductivity of Ba_3N (chain and bulk), Ba_3NSb and Ba_3NBi: along x (cross-chain; dashed curves) and z (along the chains; solid curves). (b) The accumulation of thermal conductivity (κ_{accum}) along the chain direction as a function of frequency for each system at RT. The bulk systems have similar cross-chain thermal conductivities.

As with carbon nanotubes[39] and graphene[8,47], the flexure branches $(\ell = 1, j = 1)$ and $(\ell = 1, j = 2)$ give significant contributions (31% at RT) to the overall thermal conductivity, despite having low velocity phonons. The linear acoustic branches $(\ell = 0, j = 1)$ and $(\ell = 0, j = 2)$ contribute only ~10% to the total κ. More interestingly, a high frequency optic branch $(\ell = 0, j = 12)$ gives more than half the total κ at RT, partly due to having the highest velocity phonons (as large as 6150 m/s,

nearly twice that of the LA sound speed) and partly due to larger lifetimes. This is seen in the large increase in κ accumulation (κ_{accum}) at ~8 THz in **Figure 3(b)** which gives the RT κ_{accum} with frequency (sum of κ contributions from phonons with frequency less than a reference frequency). The highest frequency modes are determined by the lightest atoms (N) vibrating in the stiffest direction (along *z*). As the phonon selection rules discussed above particularly apply to these vibrations, these modes have less scattering and longer lifetimes. Furthermore, at the Γ point in Fig. 2(a) the $(\ell = 1, j = 12)$ mode has the highest frequency (nearest neighbor N atoms vibrating out-of-phase) and the $(\ell = 0, j = 12)$ has the lower frequency (all N atoms vibrating in-phase). At the A point these vibrations become degenerate with intermediate frequency due to the phase factors in Eq. 1, with half the N atoms not vibrating and the second nearest neighbor N atoms vibrating out-of-phase. The large difference between the Γ and A frequencies for these branches results in highly dispersive phonons. Large optic phonon contributions to κ are rare as these branches often have less dispersion than heat-carrying acoustic modes. However, they have been found to be important in $Ge_2Sb_2Te_5$ [48] and functionalized graphane [49]. As the $(\ell = 0, j = 12)$ optic branch lies at higher frequencies than the other heat-carrying modes, phonon-defect interactions [50-52] may be an important resistive process in single chain Ba_3N, and the percentage of their contributions are suppressed at lower temperatures.

Bulk Ba_3N — Bulk Ba_3N has a trigonal chain pattern in the *xy* plane with lattice parameters *a* = 7.642 Å and *c* = 7.050 Å [53] (**Figure 1(a)**). As demonstrated by the electronic charge density in **Figure 1(c)** and the near quadratic behavior of the transverse acoustic branches along the Γ-A direction in **Figure 2(c)**, the chains are only weakly coupled in bulk Ba_3N. The full phonon dispersions are given in Figure S2 in the Supplemental Material [43]. Despite the weakness of these interactions, chain coupling breaks the symmetry-based selection rules for phonon-phonon scattering present in an isolated chain. This gives more scattering of heat-carrying modes resulting in lower κ as seen in **Figure 3**, $\kappa_{chain}/\kappa_{bulk,z}$~3 at RT. Similar dimensional reductions of κ were demonstrated for polyethylene

($\kappa_{chain}/\kappa_{bulk,z}$~3 [27,54]) and for graphene compared to graphite, $\kappa_{graphene}/\kappa_{in\text{-}plane,graphite}$~1.6 [6,55]. The calculations presented here for bulk Ba_3N and Ba_3NX do not explicitly incorporate vdW interactions as these give similar vibrational behaviors (Figure S3 in Supplemental Material [43]).

Regarding the anisotropy, in-chain bonds are primarily ionic with in-chain Ba-N bond lengths 2.744 Å, while the chains are weakly coupled in bulk Ba_3N with the smallest chain-chain bond length being 4.843 Å. This bonding discrepancy results in softer phonon dispersions along cross-chain directions (Γ→M→K→Γ) than along the chains (Γ→A) in Ba_3N and Ba_3NSb (**Figure 1**), resulting in higher phonon speeds along the chains. For example, the LA sound speeds for bulk Ba_3N are v_{LA}(Γ→M) = 2433 m/s and v_{LA}(Γ→A) = 3512 m/s. As a result of this directional variation, κ_z/κ_x~7.5 at RT for bulk Ba_3N and $\kappa_z > \kappa_x$ over the entire temperature range in **Figure 3(a)**. κ_{accum} along the chain direction (z) for bulk Ba_3N shown in **Figure 3(b)** demonstrates distinct step-like contributions to the overall κ in small, discrete frequency ranges (also found in Ba_3NX systems, though to a lesser degree). These discrete κ_{accum} jumps can be correlated with sections of the phonon dispersion in **Figure 2(c)** where optic branches are strongly dispersive along the Γ→A direction (large velocities) and flat in the Γ→M→K→Γ directions (large density of states (DOS)). These optic mode contributions give only ~10% of the total κ_z in bulk Ba_3N, much less than the optic contributions in single chain Ba_3N.

Bulk Ba_3NX — Heavy Sb and Bi atoms have been separately intercalated into the bulk Ba_3N chain structure to create Ba_3NX (X=Sb, Bi) crystals [56] (see **Figure 1(b)**). For Ba_3NSb (Ba_3NBi), the lattice parameters a=7.534 (7.611) Å and c=6.643 (6.679) Å are smaller than those of Ba_3N (a = 7.642 Å and c = 7.050 Å). The smallest chain-chain bond length is also reduced to 3.876 (3.949) Å [56] mostly due to a π/6 rotation of the chains with respect to those of Ba_3N. The stronger chain bonding and reduced volume in bulk Ba_3NX gives an overall higher frequency dispersion (see **Figure 2(d)** for Ba_3NSb) and increased sound speeds over those found in bulk Ba_3N alone: for Ba_3NSb v_{LA}(Γ→M) = 3416 m/s and v_{LA}(Γ→A) = 3966 m/s and for Ba_3NBi v_{LA}(Γ→M) = 3145 m/s and v_{LA}(Γ→A) = 3751 m/s. Thus,

reduced volume gives stronger bonding and stiffer phonon frequencies in bulk Ba_3NX compared with Ba_3N and enhanced thermal transport is therefore expected in the Ba_3NX systems.

However, this is not the case as $\kappa_{Ba_3N} > \kappa_{Ba_3NX}$ in the *z* direction while κ_x are comparable for the bulk materials. This is largely due to the interplay of (1) increased interchain bonding (giving increased κ) and (2) low-frequency *X* atom vibrations acting as scattering channels for the heat-carrying acoustic phonons (giving reduced κ). **Figure 2(e)** gives the DOS projected on the Sb vibrations in Ba_3NSb, which demonstrate prototypical Einstein oscillator behavior - strongly peaked DOS in a narrow frequency range. The additional low-lying, flat optic branches contribute little to heat flow and suppress the effect of increased acoustic velocities in Ba_3NX. To further elucidate this interplay, we numerically removed all scatterings involving Sb vibrations in the calculation of κ for Ba_3NSb, while retaining all other physical features. Removing these scatterings gives two times larger κ_z and three times larger κ_x in Ba_3NSb. The heavy Sb/Bi atoms play dual roles: increasing κ via an enhancement of phonon velocities and decreasing κ via a reduction of phonon lifetimes from new scattering channels.

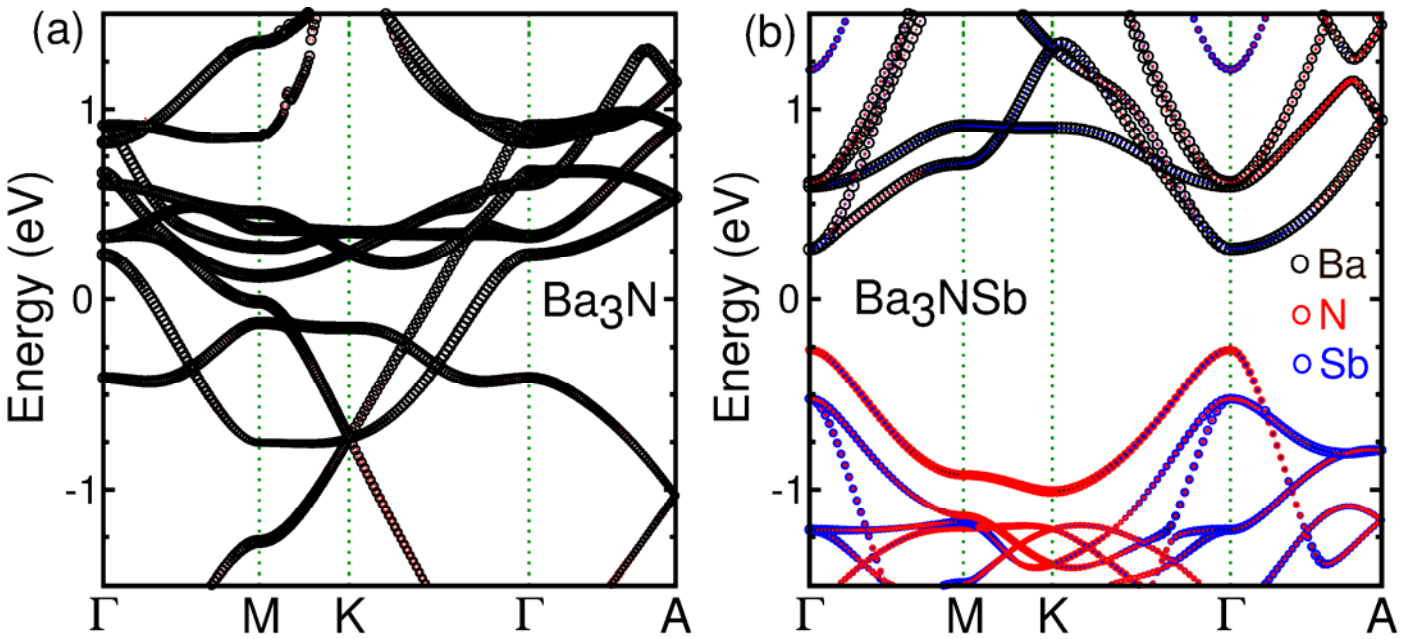

Figure 4: Atom projected electronic band structure for bulk (a) Ba_3N (metallic) and (b) Ba_3NSb (semiconductor, 0.5 eV bandgap). Black, red, and blue circles indicate individual atomic contributions from Ba, N, and Sb atoms, respectively. The sizes of the circles are proportional to the individual contributions.

Electronic properties — The structural symmetry discussed above governs not only the vibrational and transport properties of Ba_3N, but also the electronic properties. As discussed in a recent study, the quasi 1D nature of bulk Ba_3N gives rises to a unique band topology suitable for electride applications[30]. The calculated band structures of Ba_3N and Ba_3NSb are shown in **Figures 4(a)** and **4(b)**, respectively. As demonstrated there, Ba_3N is metallic, however, Ba_3NSb and Ba_3NBi (not shown) have large band gaps ~0.5-0.6 eV in qualitative agreement with experimental observations[56]. Based on the valence electrons, the chemical formula of bulk Ba_3N can be described as $(Ba^{2+})_3N^{3-}3e^-$, with the extra three electrons confined between the 1D chains. For Ba_3NX, these are taken up by the X atoms to give a closed shell configuration: $(Ba^{2+})_3(N^{3-})(X^{3-})$. As shown in **Figure 4(b)**, the conduction bands of Ba_3NSb are predominantly determined by the unoccupied 4*d* states of the Ba atoms with some mixing with the 5*s* Ba orbitals and the 2*p* N orbitals. The valence bands, by contrast, exhibit hybridization between all three atom types.

Conclusions — We unravel the roles of composition, structure, symmetry and dimensionality on vibrational properties and transport, particularly applied to Ba_3N-derived materials. The underlying symmetry of single chain Ba_3N gives chirality to the phonons and limits their interactions, driving the lattice thermal conductivity (κ) higher compared to bulk and giving an unusual contribution to κ from high-frequency optical modes. Despite weak chain coupling in bulk Ba_3N, this material breaks symmetry-based selection rules for phonon-phonon scattering in the single chain and gives a κ value ~3 times smaller. Strong in-chain bonding compared with weak van der Waals bonding between chains also yields significant κ anisotropy in the bulk materials. The addition of intercalating large, heavy atoms (X=Sb, Bi) in the bulk Ba_3N structure gives rise to competing effects: (i) compressed cell volume and stiffer phonon frequencies enhancing κ, and (ii) nearly dispersionless, low-frequency scattering

channels that suppress κ. The net result is a reduction in κ for Ba_3NX compared to bulk Ba_3N. Ba_3N is metallic, while Ba_3NX compounds are semiconducting despite having similar structures. The physical insights derived here are general to a large class of 1D and quasi-1D materials and will guide future calculations and measurement interpretation of vibrational behavior and thermal transport in these. In particular, we derived new symmetry constraints for thermal resistance and elucidate the unusual role of intercalating atoms in weakly bonded structures.

Acknowledgements:

We acknowledge support from the U. S. Department of Energy, Office of Science, Basic Energy Sciences, Materials Sciences and Engineering Division. This research used resources of the Compute and Data Environment for Science (CADES) at the Oak Ridge National Laboratory, which is supported by the Office of Science of the U.S. Department of Energy under Contract No. DE-AC05-00OR22725. The Department of Energy will provide public access to these results of federally sponsored research in accordance with the DOE Public Access Plan.

References:

[1] P. Bharadwaj and L. Novotny, Optics and Photonics News **26**, 24 (2015).
[2] A. Gupta, T. Sakthivel, and S. Seal, Progress in Materials Science **73**, 44 (2015).
[3] D. H. Cao, C. C. Stoumpos, O. K. Farha, J. T. Hupp, and M. G. Kanatzidis, Journal of the American Chemical Society **137**, 7843 (2015).
[4] F. Torrisi and J. N. Coleman, Nature nanotechnology **9**, 738 (2014).
[5] D. Akinwande, N. Petrone, and J. Hone, Nature communications **5**, 5678 (2014).
[6] G. Fugallo, A. Cepellotti, L. Paulatto, M. Lazzeri, N. Marzari, and F. Mauri, Nano letters **14**, 6109 (2014).
[7] A. Alofi and G. Srivastava, Physical Review B **87**, 115421 (2013).
[8] J. H. Seol *et al.*, Science **328**, 213 (2010).
[9] X. Gu, B. Li, and R. Yang, Journal of Applied Physics **119**, 085106 (2016).
[10] J. Liu, G.-M. Choi, and D. G. Cahill, Journal of Applied Physics **116**, 233107 (2014).
[11] C. Muratore *et al.*, Applied Physics Letters **102**, 081604 (2013).
[12] Y. Kuang, L. Lindsay, S. Shi, X. Wang, and B. Huang, International Journal of Heat and Mass Transfer **101**, 772 (2016).
[13] Y. Kuang, L. Lindsay, S. Shi, and G. Zheng, Nanoscale **8**, 3760 (2016).
[14] Z. Wei, F. Yang, K. Bi, J. Yang, and Y. Chen, The Journal of Physical Chemistry C (2018).
[15] G. Zhu, J. Liu, Q. Zheng, R. Zhang, D. Li, D. Banerjee, and D. G. Cahill, Nature communications **7**, 13211 (2016).
[16] X. Qian, X. Gu, M. S. Dresselhaus, and R. Yang, The journal of physical chemistry letters **7**, 4744 (2016).

[17] A. Lipatov, P. M. Wilson, M. Shekhirev, J. D. Teeter, R. Netusil, and A. Sinitskii, Nanoscale **7**, 12291 (2015).
[18] J. O. Island *et al.*, Advanced Materials **27**, 2595 (2015).
[19] G. Liu, S. Rumyantsev, M. A. Bloodgood, T. T. Salguero, M. Shur, and A. A. Balandin, Nano letters **17**, 377 (2016).
[20] M. A. Stolyarov *et al.*, Nanoscale **8**, 15774 (2016).
[21] G. Yumnam, T. Pandey, and A. K. Singh, The Journal of Physical Chemistry C (2018).
[22] T. Pandey, D. S. Parker, and L. Lindsay, Nanotechnology **28**, 455706 (2017).
[23] G. Qin, X. Zhang, S.-Y. Yue, Z. Qin, H. Wang, Y. Han, and M. Hu, Physical Review B **94**, 165445 (2016).
[24] Y. Liu *et al.*, Scientific Reports **7**, 43886 (2017).
[25] X. Wu, V. Varshney, J. Lee, T. Zhang, J. L. Wohlwend, A. K. Roy, and T. Luo, Nano letters **16**, 3925 (2016).
[26] J. Carrete, W. Li, L. Lindsay, D. A. Broido, L. J. Gallego, and N. Mingo, Materials Research Letters **4**, 204 (2016).
[27] A. Henry, G. Chen, S. J. Plimpton, and A. Thompson, Physical Review B **82**, 144308 (2010).
[28] X. Chen *et al.*, Nature communications **6**, 6723 (2015).
[29] Q. Zhang *et al.*, ACS nano **12**, 2634 (2018).
[30] C. Park, S. W. Kim, and M. Yoon, Physical Review Letters **120**, 026401 (2018).
[31] H. Zhu *et al.*, Science **359**, 579 (2018).
[32] X. Xu, W. Zhang, J. Wang, and L. Zhang, Journal of Physics: Condensed Matter **30**, 225401 (2018).
[33] L. Zhang and Q. Niu, Physical review letters **115**, 115502 (2015).
[34] L. Lindsay, D. Broido, and N. Mingo, Physical Review B **80**, 125407 (2009).
[35] V. Popov, V. Van Doren, and M. Balkanski, Physical Review B **61**, 3078 (2000).
[36] G. Mahan and G. S. Jeon, Physical Review B **70**, 075405 (2004).
[37] A. Calzolari, T. Jayasekera, K. W. Kim, and M. B. Nardelli, Journal of Physics: Condensed Matter **24**, 492204 (2012).
[38] L. Lindsay and D. Broido, Physical Review B **81**, 205441 (2010).
[39] L. Lindsay, D. Broido, and N. Mingo, Physical Review B **82**, 161402 (2010).
[40] W. Li, J. Carrete, N. A. Katcho, and N. Mingo, Computer Physics Communications **185**, 1747 (2014).
[41] L. Lindsay, D. Broido, and T. Reinecke, Physical review letters **109**, 095901 (2012).
[42] L. Lindsay, D. Broido, and T. Reinecke, Physical Review B **88**, 144306 (2013).
[43] *See Supplemental Material at http://link.aps.org/supplemental/ for details calculations deatils, convergence tests, and full phonon dispersions.*
[44] S.-i. Tamura, Physical Review B **27**, 858 (1983).
[45] S.-i. Tamura, Physical Review B **30**, 849 (1984).
[46] J. M. Ziman, *Electrons and phonons: the theory of transport phenomena in solids* (Oxford university press, 1960).
[47] L. Lindsay, D. Broido, and N. Mingo, Physical Review B **82**, 115427 (2010).
[48] S. Mukhopadhyay, L. Lindsay, and D. J. Singh, Scientific reports **6**, 37076 (2016).
[49] L. Lindsay and Y. Kuang, Physical Review B **95**, 121404 (2017).
[50] C. Polanco, Phys. Rev. B **97**, 014303 (2018).
[51] C. A. Polanco and L. Lindsay, Physical Review B **98**, 014306 (2018).
[52] Q. Zheng, C. A. Polanco, M.-H. Du, L. R. Lindsay, M. Chi, J. Yan, and B. C. Sales, Physical Review Letters **121**, 105901 (2018).
[53] U. Steinbrenner and A. Simon, Zeitschrift für anorganische und allgemeine Chemie **624**, 228 (1998).
[54] N. Shulumba, O. Hellman, and A. J. Minnich, Physical review letters **119**, 185901 (2017).
[55] L. Lindsay, D. Broido, and N. Mingo, Physical Review B **83**, 235428 (2011).
[56] F. Gäbler, M. Kirchner, W. Schnelle, U. Schwarz, M. Schmitt, H. Rosner, and R. Niewa, Zeitschrift für anorganische und allgemeine Chemie **630**, 2292 (2004).